ACS APPLIED BIO MATERIALS

www.acsabm.org

Forum Article

Bioactive Fibronectin-III$_{10}$–DNA Origami Nanofibers Promote Cell Adhesion and Spreading

Alex Buchberger,[‡] Kyle Riker,[‡] Julio Bernal-Chanchavac, Raghu Pradeep Narayanan, Chad R. Simmons, Nour Eddine Fahmi, Ronit Freeman,[*] and Nicholas Stephanopoulos[*]

Cite This: https://doi.org/10.1021/acsabm.2c00303

Read Online

ACCESS | Metrics & More | Article Recommendations | Supporting Information

ABSTRACT: The integration of proteins with DNA nanotechnology would enable materials with diverse applications in biology, medicine, and engineering. Here, we describe a method for the incorporation of bioactive fibronectin domain proteins with DNA nanostructures using two orthogonal coiled-coil peptides. One peptide from each coiled-coil pair is attached to a DNA origami cuboid in a multivalent fashion by attaching the peptides to DNA handles. These structures can then be assembled into one-dimensional arrays through the addition of a fibronectin domain linker genetically fused with the complementary peptides to those on the origami. We validate array formation using two different self-assembly protocols and characterize the fibers by atomic force and electron microscopy. Finally, we demonstrate that surfaces coated with the protein–DNA nanofibers can serve as biomaterial substrates for fibroblast adhesion and spreading with the nanofibers showing enhanced bioactivity compared to that of the monomeric protein.

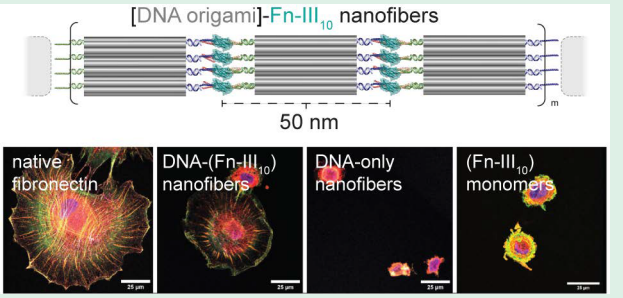

KEYWORDS: *DNA nanotechnology, coiled-coils, self-assembly, biomaterials, fibronectin, bionanotechnology, supramolecular chemistry*

INTRODUCTION

The ability to control the morphology, size, and activity of biomimetic structures is a long-standing goal of nanotechnology. DNA, in particular, allows for the construction of complex and highly addressable nanostructures through the self-assembly of multiple synthetic oligonucleotides with unique sequences.[1−3] Recently, there has been a great focus on the functionalization of these structures with peptides[4,5] or proteins[6−8] to impart a biological function or to diversify their structural and chemical properties. One area where hybrid protein–DNA nanomaterials have found application is in the creation of cell-engaging substrates for probing, or controlling, cell adhesion and biological activity. For example, a number of reports have used DNA nanostructures functionalized with peptides or proteins to probe the effect of ligand spacing, on cell activity, or as force sensors for cell receptor–substrate interactions.[9−14] Less common is the use of polypeptide-modified DNA nanoscaffolds as mimics of fibrous extracellular matrix (ECM) proteins like fibronectin (Fn) or collagen. Silver and co-workers reported that DNA ribbons decorated with the 10th type III Fn domain (Fn-III$_{10}$) could be used to tune the stiffness and thus the cell response of a substrate,[15] whereas Stupp and co-workers reported that DNA nanotubes bearing the (Fn-III$_{10}$)-derived cell-adhesive peptide RGDS could enhance neural stem cell differentiation into neurons.[16] These examples highlight the potential of probing the structure–function relationships in the ECM by tuning the diameter and mechanical properties of a fiber independently of the bioactive components attached to it. However, to fully realize this potential, new methods to incorporate the bioactive proteins directly into a nanostructure in a highly biomimetic fashion are necessary.

In particular, we were inspired by the molecular structure of native fibronectin, which is composed of multiple bioactive modules linked together like beads on a string and helps mediate cell attachment, migration, and differentiation.[17,18] We asked whether a protein–DNA nanofiber could recapitulate the linear presentation and regular spacing of Fn-III$_{10}$, which is displayed with a periodic spacing of ∼50 nm (Figure 1A). Fn-III$_{10}$ binds to integrin receptors on cells and mediates their attachment to the extracellular matrix.[17,19,20] The ability to independently control such a nanofiber's morphology (through the DNA origami component) and bioactivity (through the protein attached to them) could be useful for applications in tunable biomaterials or for fundamental cell–matrix studies.[21] Toward this end, we sought to use a DNA origami cuboid scaffold[22] to recapitulate this protein spacing (Figure 1B). We

Special Issue: Self-Assembling Biomaterials from Proteins, Peptides, and DNA

Received: April 2, 2022
Accepted: September 1, 2022

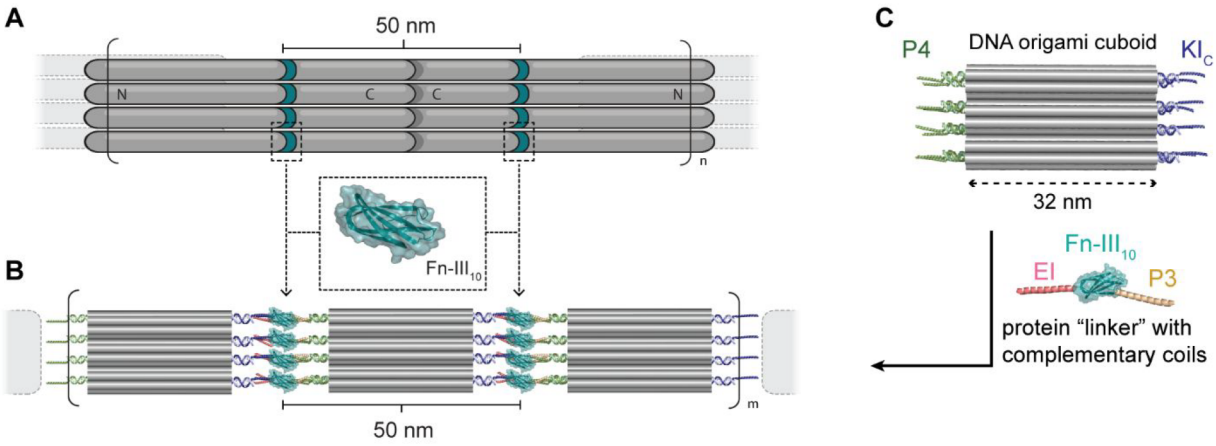

Figure 1. Overview of approach. (A) Native fibronectin spaces the 10th type III domain (Fn-III$_{10}$; in green) ~50 nm apart. (B) This arrangement can be recapitulated with DNA origami nanostructures that position that same domain with a similar spacing (bottom). (C) Hybrid protein−origami nanofibers can be synthesized through the self-assembly of a DNA cuboid bearing two orthogonal coiled-coils (P4 and KI$_c$) that are complementary to coils genetically fused to the Fn-III$_{10}$ domain (P3 and EI, respectively). Each origami interface is mediated by eight protein linkers.

reasoned that to best mimic its physiological arrangement in the native protein, where individual domains are linked in series like beads on a string, the Fn-III$_{10}$ proteins should be linked to the origami scaffolds at the two termini.

Rather than covalently attaching DNA handles to the protein,[4,5,8] which is especially difficult if two distinct attachment sites are desired, as in this case, we instead designed an approach relying on coiled-coil self-assembly. Recently, we reported that the cuboid nanostructures could be assembled into long, one-dimensional arrays through multivalent coiled-coil peptide interactions.[23] We reasoned that it might be possible to incorporate proteins into these systems by using two orthogonal coiled-coil pairs (termed P3/P4[24] and EI/KI[23,25]). In this design, we genetically fused P3 and EI to the Fn-III$_{10}$ protein and separately linked the P4 and KI peptides to opposite sides of the origami through peptide−DNA conjugates (Figure 1C). Because our approach relies on the selective self-assembly of these coiled-coil pairs, it requires no additional manipulation of the protein prior to self-assembly with the peptide-bearing origami. As a result, we can avoid chemically conjugating DNA to the protein, which usually requires purification from under-modified species, resulting in a marked decrease in the yield of the final species. Our approach should also position the Fn-III$_{10}$ domains in a consistent orientation at each junction and throughout the fiber. We demonstrate the successful assembly and characterization of the hybrid protein−DNA nanofibers and show that they can promote greater fibroblast spreading in comparison with the nonassembled Fn-III$_{10}$ domain alone, while cell adhesion seemed to be comparable. This suggests that the fibrillar morphology as well as the spacing of the Fn-III$_{10}$ within the nanofiber are important parameters that guide cell spreading and that hybrid origami−protein nanostructures are a promising novel biomaterial that can provide unique handles to tune these factors and test their effects on cell behavior.

MATERIALS AND METHODS

Peptide Synthesis and Characterization. Peptides were made on a CEM Liberty Blue instrument using standard solid-phase peptide synthesis (SPPS) with Fmoc-protected amino acids, as previously reported.[3] Peptides were synthesized at a 0.1 mmol scale on Rink-Amide resin (0.57 mmol/g). Deprotection steps were performed in 20% piperidine in dimethyl formamide (DMF). Coupling was carried out using *N*,*N*′-diisopropylcarbodiimide (DIC), Oxyma, and Fmoc-protected amino acids at 5 mol equiv to the resin. All peptides were capped using acetic anhydride and *N*,*N*-diisopropylethylamine (DIPEA). Peptides were cleaved from the resin in a 10 mL solution of a 95:2.5:2.5 ratio of trifluoroacetic acid (TFA), triisopropylsilane (TIPS), and water. The peptide was precipitated from the cleavage solution using 40 mL of cold diethyl ether. The precipitate was centrifuged, and the supernatant was discarded. The peptide pellets were dissolved in a 70:30 mixture of water and acetonitrile with 0.1% TFA for purification. All peptides were purified by reverse phase chromatography on a Waters HPLC with a C18 Phenomenex column using a linear gradient of buffer B (acetonitrile + 0.1% TFA) in buffer A (water + 0.1% TFA) at a rate of a 1.5% increase in buffer B per min. Peptide identity and purity were confirmed via MALDI-TOF MS on an AB SCIEX 4800 MALDI TOF/TOF using a matrix of α-cyano-4-hydroxycinnamic acid matrix (Sigma).

Synthesis of Peptide−DNA Conjugates. Peptides were conjugated to DNA following previously reported protocols[3] using strain-promoted azide−alkyne cycloaddition (SPAAC). Briefly, DNA was first coupled to DBCO by mixing amine modified strands at a concentration of 1 mM with 5 mol equiv of DBCO-sulfo-NHS in phosphate buffered saline (PBS) consisting of 10 mM Na_2HPO_4, 1.8 mM K_2HPO_4, 136 mM NaCl, and 2.7 mM KCl, pH = 8.0. To remove excess DBCO, the reaction was washed four times using a 3 kDa MWCO filter. DBCO-modified DNA was reacted with the azide modified peptide at room temperature and shaken overnight. All peptides besides KI were reacted at a 2:1 ratio with the DNA; KI peptides were reacted at a 1:1 ratio to avoid precipitation due to electrostatic complexation. All reactions were syringe filtered with a 0.22 μm filter prior to purification. The reaction mixtures were purified via reverse phase HPLC on an Agilent 1220 Infinity using a Zorbax Eclipse XDB-C18 column with a gradient of 10% to 100% methanol in 50 mM triethylammonium acetate (TEAA) over 60 min. The synthesis was confirmed by MALDI-TOF mass spectrometry using a matrix of 3-hydropicolinic acid (HPA, Sigma).

Expression of P3−Fn-III$_{10}$−EI Protein. All primers and oligonucleotides were purchased from Integrated DNA Technologies, Inc. (Coralville, IA). The gene for P3-(Fn-III10)-EI fusion protein was inserted in the pQE-80L plasmid via Gibson Assembly. The constructed plasmid was transformed into *E. coli* DH5α competent cells, from New England Biolab, Inc. USA (Rowley, MA) for plasmid amplification. The plasmids were purified via a miniprep kit from Qiagen (Hilden, Germany). After plasmid purification, all mutant constructs were verified via Sanger DNA sequencing, using primers: pBR-Eco-FWD: aataggcgtatcacgaggc; T0-Term-REV:

https://doi.org/10.1021/acsabm.2c00303
ACS Appl. Bio Mater. XXXX, XXX, XXX−XXX

GCGGCAACCGAGCGTTC. The plasmids were then transformed into BL21 (DE3) cells, from New England Biolab, Inc. (Rowley, MA) for protein expression. The transformed cells were grown in 1× Luria Bertani (LB) broth containing 100 g/mL carbenicillin at 37 °C to an OD600 = 0.6−1.0. Once the optimal OD level was reached, the culture was induced with 1.0 mM isopropyl-D-thiogalactopyranoside (IPTG) (SigmaAldrich, St. Louis, MO) and allowed to grow overnight at 18 °C. The overnight culture was harvested by centrifugation at 4200 rpm for 10 min. The cell pellets were resuspended in 15 mL of lysis buffer containing 25 mM Tris, pH = 8.0, 150 mM NaCl, and 0.1 mM EDTA supplemented with 100 μL of 100 mM PMSF, 50 μL of DNase l (10 mg/mL), and 50 μL of lysozyme (10 mg/mL) and lysed using sonication. The cell lysate was subsequently centrifuged at 15 000 rpm for 30 min to remove cell debris, loaded onto a 1 mL HisTrap HP Ni-NTA column (GE Healthcare, USA), and washed with 10 column volumes of 50 mM Tris, pH = 8.0, 300 mM NaCl, and 10 mM imidazole to remove nonspecifically bound molecules. The target protein was eluted with a 40 column volume stepwise gradient using an elution buffer composed of 50 mM Tris, pH = 8.0, 150 mM NaCl, and 500 mM imidazole. The stepwise gradient consisted of 10 column volumes of 10% of the elution buffer and then a linear gradient from 10% to 100% elution buffer over 30 column volumes. Peak fractions were analyzed via SDS-PAGE; the fractions containing the target protein were consolidated and placed in a 10 kDa molecular weight cutoff (MWCO) dialysis membrane, and the sample was dialyzed overnight at 4 °C against 1 L of 50 mM Tris-HCl buffer with 0.5 mM EDTA, pH = 8.0. The resulting sample was concentrated using an Amicon 10 kDa (MilliporeSigma, USA) MWCO filter. The TEV fusion protein was cleaved with TEV protease at a 50:1 ratio and allowed to sit overnight at room temperature. The cleaved protein was loaded onto a 1 mL HisTrap HP Ni-NTA column, and the flowthrough was collected. To further remove residual MBP, the protein sample was loaded onto a 1 mL MBPTrap HP column (GE Healthcare, USA) and the resulting flowthrough was collected. The flowthrough was placed in a 10 kDa MWCO dialysis membrane, dialyzed overnight at 4 °C against 1 L of PBS buffer, and then concentrated using an Amicon 10 kDa (MilliporeSigma, USA) MWCO filter.

Preparation of Surfaces Modified with DNA−Fn-III$_{10}$ Nanofibers. Coverslips were submerged in a solution of 2% Micro-90 in DI water at 60 °C for 30 min. Coverslips were then rinsed six times with DI water and twice with ethanol and allowed to dry completely. After drying, coverslips were plasma cleaned (Basic Plasma Cleaner, Harrick Plasma) for 5 min on high. Glass bottom dishes (supplied sterile from the manufacturer) were plasma cleaned directly with no additional preparation. For improved consistency, initial surface coatings were applied within 15 min of plasma cleaning.

DNA Origami Cuboid Annealing Protocol and Characterization. DNA origami samples were annealed using two distinct protocols: (1) one-pot annealing; (2) hierarchical (two-step) annealing and incubation. The one-pot annealing method was used for samples A−E in Figure S6 (corresponding to lanes 1−5 in Figure S7 and lanes 1−5 in Figure S8). Samples were made at 10 nM relative to the M13 scaffold with 10 equiv of staple strands and 80 equiv of peptide−DNA conjugates (equimolar with the eight handles per origami). Samples were heated in a PCR thermocycler at 65 °C for 15 min followed by a 0.5 °C/min temperature ramp from 60 to 40 °C and finally rapid cooling to 4 °C to avoid undesired nonspecific blunt-end stacking. The two-step protocol was used for sample F in Figure S6 (corresponding to lane 6 in Figure S7) and all samples incorporating proteins. This protocol consisted of the same procedure for the initial origami annealing, followed by a second incubation at room temperature. All protein added was equimolar to the peptide−DNA handles (i.e., 80 equiv relative to the M13 scaffold strand). All DNA origami were analyzed by a 1% agarose gel electrophoresis (AGE). The gels were prestained with ethidium bromide, electrophoresed at 80 V for 1 h, and then imaged with a Bio-Rad Molecular Imager GelDOC XR+ imaging system. Arrays of origami linked by P3−Fn-III$_{10}$−EI were purified utilizing Amicon 100 kDa molecular weight cutoff filters. The samples were centrifuged at 8000 rpm for 5 min, followed by the addition of fresh buffer, for a total of four times.

Atomic Force Microscopy (AFM) Characterization. AFM images were obtained using a Veeco DI MultiMode V instrument in air using scan assist mode with SCANASYST-AIR tips (Bruker). Two μL of sample and 48 μL of 1× TAE with 12.5 mM Mg^{2+} buffer were pipetted onto freshly cleaved mica and allowed to adhere to the surface for 2 min. Samples were washed with 50 μL of water to remove excess salts and immediately dried with a stream of air.

Transmission Electron Microscopy (TEM) Characterization. All TEM images were collected using a Philips CM-12 transmission electron microscope. DNA origami−peptide arrays were adsorbed onto glow-discharged Formvar copper mesh grids (Ted Pella) and stained with a solution of 2% uranyl acetate in water.

Surface Functionalization. Immediately following plasma cleaning, a sufficient volume of the desired coating solution was applied to the surface in order to achieve a final coating density of 2 pmol/cm^2 and then incubated for 1 h. Following coating, the remaining liquid on the surfaces was aspirated and surfaces were gently rinsed three times with 1× PBS. For DNA-modified surfaces, 12.5 mM $MgCl_2$ was added to all wash solutions to help maintain the surface coating.

Characterization of DNA Cuboid Nanofiber and Integrin Modified Surfaces. Glass bottom dishes were modified with DNA cuboid nanofibers as described above. Following modification, the coating was characterized using the fluorescent DNA intercalator YOYO-1 (Thermo Fisher, Y3601). Integrin binding assays were performed using a modified solid-phase binding assay.[26,27] Solutions of the recombinant human integrins α5β1 and αvβ3 (R&D systems, 3230-A5 and 3050-AV, respectively) were prepared (2 μg/mL, TS-B Buffer), added to separate DNA cuboid−nanofiber modified surfaces, and incubated for 1 h at room temperature. Following integrin binding, surfaces were washed an additional three times for 5 min in PBS-T + Mg^{2+} to remove excess integrin. Surfaces were then fixed in a solution of 4% paraformaldehyde (PFA) in PBS + 12.5 mM Mg^{2+} for 15 min to preserve bound integrin in subsequent immunofluorescent labeling.

Cell Culture. Normal human foreskin fibroblasts (HFFs) were obtained from the UNC Tissue Culture Facility (HDF-UNCH1, passage number 18) and cultured in DMEM, high glucose (Gibco, 11965092) supplemented with 10% fetal bovine serum (Seradigm, 1500-500G) and 1% penicillin−streptomycin (Gibco, 15140122). Cells were passaged every 3 days and used at a passage number between 20 and 25.

Fibroblast Adhesion Assays. For adhesion experiments, DNA−Fn-III$_{10}$ nanofiber modified surfaces (as described above) were prepared immediately before use, alongside fibronectin and P3−Fn-III$_{10}$−EI monomer-only surfaces used as positive and negative controls, respectively. HFF cells were plated on the modified surfaces at a density of 2500 cells/cm^2 in reduced serum media (DMEM, 2% FBS). Cells were allowed to adhere for 2 h and were then gently washed once with 1× PBS, followed by fixation for 15 min with 4% PFA in PBS (Invitrogen Image-iT Fixative, R37814). Following fixation, cells were washed three times with ice-cold PBS + Mg^{2+} (1× PBS, 5 mM $MgCl_2$).

Immunocytochemistry. The following primary antibodies and their dilutions were used for immunocytochemistry: mouse anti-vinculin (1:500, Sigma-Aldrich V9131), rabbit anti-β3/CD61 [SJ19-09] (1:500, Invitrogen MA5-32077), and rat anti-β1 [MB1.2] (1:100, Sigma MAB1997).

Following fixation, cells on the modified surfaces were first permeabilized for 5 min in 0.1% Triton-X100 in PBS followed by three, 5 min washes in PBS + Mg^{2+}. After permeabilization, cells were blocked with a 1% BSA Fraction V solution (Gibco, 15260037) in PBS-T + Mg^{2+} (1× PBS, 0.1% Tween-20, 5 mM Mg^{2+}) for 30 min at room temperature. The blocking solution was removed and replaced with a solution of the primary antibodies (1% BSA in PBS-T + Mg^{2+}) and incubated for 1 h at room temperature. Surfaces were then washed three times for 5 min in PBS-T + Mg^{2+}. A solution of AlexaFluor-conjugated secondary antibodies against the appropriate

https://doi.org/10.1021/acsabm.2c00303
ACS Appl. Bio Mater. XXXX, XXX, XXX−XXX

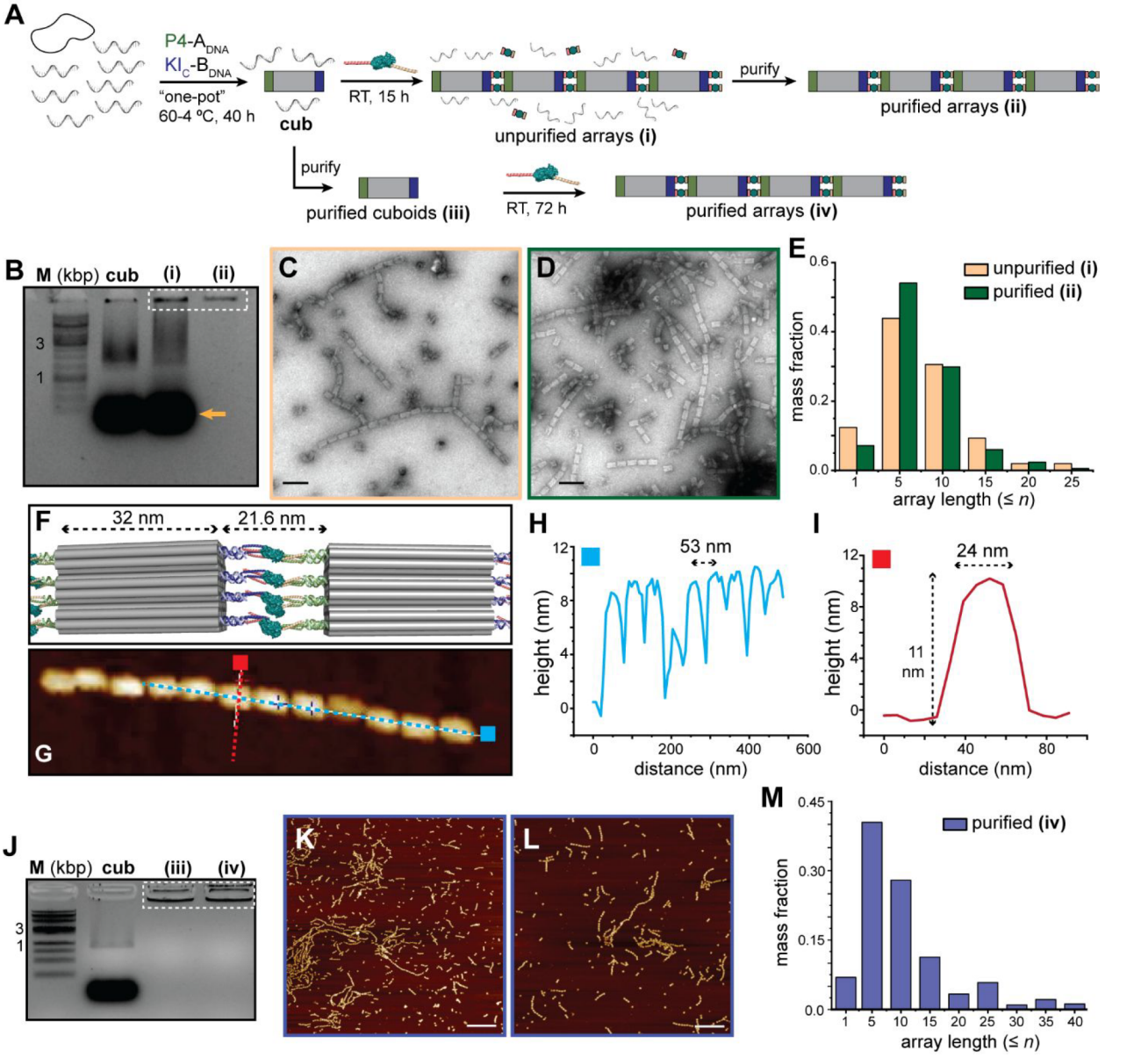

Figure 2. Formation of 1D fibronectin−origami arrays using coiled-coil linkers. (A) Two different protocols for assembling protein−DNA nanofibers, where (i−iv) indicates the samples referred to below. (B) Agarose gel electrophoresis of samples. Lane M: dsDNA ladder (kbp); cub: cuboids with peptides after one-pot annealing; (i): sample after addition of protein linkers and incubation at 37 °C; (ii): purified protein−DNA fibers. The white box denotes the high-molecular weight aggregates that correspond to the nanofibers. The orange arrow indicates excess free staples and peptide−DNA conjugates. (C, D) Negative stain TEM images of the unpurified (tan) and purified (green) protein−DNA fibers. Scale bars: 100 nm. (E) Histogram of the array length for samples (i) and (ii). (F) Schematic of protein−DNA nanofiber interface with the expected dimensions indicated. (G) AFM zoom-in image of an isolated protein−DNA fiber. (H, I) AFM height profiles along the blue and red line, respectively, from (G). (J) Agarose gel electrophoresis of samples. Lane M: dsDNA ladder (kbp); cub: cuboids without peptides (for comparison); (iii): cuboids with peptides following purification; (iv): assembly of fibers from purified cuboids. The white box denotes the high-molecular weight aggregates that correspond to nonspecific aggregates for (iii) and nanofibers for (iv). (K, L) AFM images of sample (iv). (M) Histogram of array length for sample (iv). For all histograms, numbers correspond to arrays with a length equal to that between the value of the previous bin and indicated number, e.g., "10" indicates arrays 6−10 cuboids in length.

species for the primary antibodies was added to the surfaces and incubated for 1 h in the dark at room temperature. Following incubation with secondary antibodies, surfaces were washed three times with PBS-T + Mg^{2+} followed by a 1 h incubation with AlexaFluor 488-Phalloidin (1:400, Invitrogen, A12379) and a 20 min incubation with Hoechst 33342 (1:2000, Invitrogen H3570). Surfaces were washed a final three times with PBS + Mg^{2+}, then mounted on glass slides using ProLong Diamond Antifade Mountant (Invitrogen, P36965), and allowed to cure for >6 h in the dark at room temperature prior to imaging. For low magnification images and quantification, coverslips were imaged on a GE INCell Analyzer 2200 high-content microscope.

Confocal Microscopy. Confocal images were acquired on either a Zeiss LSM 710 or a Zeiss LSM 880 equipped with an Airyscan Superresolution detector. Zeiss Plan Apochromat 1.4 NA oil objectives with either 40× (LSM 710) or 63× (LSM 880) magnification were used. Power and gain settings were optimized for each fluorophore but kept consistent across similar samples.

ImageJ and Statistical Analysis. Morphometric and quantitative analysis of images and all related quantifications were performed using

https://doi.org/10.1021/acsabm.2c00303
ACS Appl. Bio Mater. XXXX, XXX, XXX−XXX

Fiji ImageJ software (National Institute of Health). Data from ImageJ was compiled using Microsoft Excel. Statistical analysis was performed using Graphpad Prism 9 software. For the determination of statistical significance, a Student's *t* test or ordinary one-way ANOVA was implemented.

RESULTS AND DISCUSSION

The monomeric protein "linker" was recombinantly expressed in *E. coli* as a genetic fusion with the P3 peptide at the N-terminus and the EI peptide at the C-terminus to yield P3−Fn-III_{10}−EI. We coupled the P4 and KI peptides (which form parallel heterodimer coiled-coils with P3 and EI, respectively) to two unique 14-nt ssDNA handles, A_{DNA} and B_{DNA}, using copper-free click chemistry with an azidolysine on the peptides.[23] These peptide−DNA conjugates could in turn be attached to the DNA origami cuboid bearing complementary handles on opposite faces. We modified the origami cuboids, which are 32 × 19.5 × 16 nm in size with sites for handle extension on the faces perpendicular to the DNA helical axes, with one or two sets of orthogonal peptides on the two smallest faces (the 19.5 × 16 nm faces). The details of protein expression and purification, peptide synthesis, and peptide−DNA conjugation, purification, and characterization can be found in Sections S2−S4.

We used circular dichroism to confirm that the P3 and P4 formed a coiled-coil, as evidenced by the characteristic peaks at 208 and 222 nm, but that no such signal was seen between these peptides and either EI or KI, demonstrating the desired orthogonality of the two pairs selected (Figure S3). Previously, we reported that DNA origami cuboids could be assembled into long, 1D arrays by functionalizing them with eight copies of the EI and KI peptides on each side,[23] so we used this same number of handles on the cuboids for all experiments herein. We also note that, in order to ensure the proper directionality of protein attachment to the peptides (Figure S5, asterisks), the B_{DNA} handle was attached to the C-terminus of the KI peptide, as opposed to our prior studies in which the handle was attached to the N-terminus. This was accomplished by moving the azidolysine that gets linked to the DNA to the C-terminus (peptide KI_C), as opposed to the N-terminus (peptide KI_N), while otherwise keeping the self-assembling motif of the peptide constant; the complete sequences for all peptides used can be found in Figure S1. We highlight that the ability to control the site specificity of DNA attachment to the peptide allows for both parallel and antiparallel coiled-coils to be used, expanding the possible design space of future materials.

We first probed whether the P3/P4 coiled-coil pair could mediate DNA nanofiber formation on its own, similar to the EI/KI_N pair.[23] We followed a "one-pot" procedure where we annealed the P3−B_{DNA} and P4−A_{DNA} conjugates with the M13 scaffold, staple strands, and staples extended with handles complementary to those on the peptides. Compared with the nanostructures lacking handles (Figure S6A), this sample yielded one-dimensional arrays of the cuboids linked along the expected interface, as imaged by negative-stain TEM (Figure S6B). In contrast, cuboids annealed with one peptide from each pair, either P4 and KI_N (Figure S6D) or P3 and EI (Figure S6E), primarily gave monomeric species indistinguishable from the unmodified cuboids. These two populations of cuboids were mixed in a second, lower-temperature annealing step to create an alternating copolymer of nanostructures, driven by *both* coiled-coil interactions (Figure S6F). Taken together, these results demonstrated that a "mixed" system of coils could sequence-specifically drive DNA nanostructure assembly, in much the same way that unique DNA sticky ends can assemble complex nanostructures.

Next, we attempted to make arrays driven by the P3−Fn-III_{10}−EI fusion (Figure 2A). We first annealed cuboids bearing P4 and KI_C, and then, in a second step, added the protein linker equimolar to the peptides in solution; i.e., 80-fold relative to the M13 scaffold due to the 10-fold excess of staples and the eight handles per cuboid face. We incubated this sample at room temperature for 15 h, a temperature that was not expected to disturb either the peptide assembly or the protein, and analyzed the sample (termed "unpurified arrays (i)" in Figure 2A) by both agarose gel electrophoresis (AGE) and negative stain TEM. As evidenced by AGE, the band corresponding to the cuboid and short oligomers transitioned to a high-molecular weight band in the loading well (Figure 2B, lanes cub vs (i)). Negative stain TEM analysis revealed 1D nanofibers (Figure 2C) with a length distribution similar to that of the sample with the mixed peptides alone (Figure S6F), including fibers of up to 26 origami in length. Thus, the protein linker bearing two coils was able to effectively assemble the DNA nanostructures and create a hybrid structure with multiple proteins interspersed between the origami cuboids and a similar efficiency to the mixed nanofibers formed solely by the two pairs of peptides.

According to AGE analysis, control experiments with cuboids bearing EI and P3 peptides incubated with P3−Fn-III_{10}−EI did not yield fibers (Figure S8), confirming that the origami must bear the complementary peptides to the handles on the protein to drive self-assembly. All of the above samples were annealed in the presence of a 10-fold excess of staples with multivalency preventing fiber "capping" and termination.[22,23] However, having an excess of peptide−DNA conjugates and protein linkers in solution could be problematic for some applications. For example, it would be counterproductive for cell studies to have an 80-fold excess of free P3−Fn-III_{10}−EI in solution, which could compete with the fibers for binding to integrin receptors. We thus explored whether the fibers could be purified ("purified arrays (ii)" in Figure 2A) using a high molecular-weight cutoff (MWCO) centrifugal filter. A 100 kDa MWCO filter should retain the fibers (as well as cuboid monomers, which are megadaltons in size) but remove free staples, peptide−DNA conjugates, and protein linkers. Indeed, after four rounds of centrifugation and dilution using this filter, no excess peptide−DNA conjugates or staples were seen by AGE (Figure 2B, lane (ii)), and long fibers were still readily observable by TEM (Figure 2D). The determination of the fiber lengths before and after purification gave virtually identical distributions (Figure 2E), demonstrating the purification did not break (or aggregate) the fibers, nor did the removal of excess peptides and proteins cause them to lengthen. It may be possible to further increase the protein−DNA fiber length using a stronger second pair of peptides than P3/P4 (e.g., on par with EI/KI), increasing the number or modifying the spatial distribution of handles, or tuning the annealing and hierarchical assembly protocol. These investigations will be the focus of a future study.

We also probed the protein−DNA nanofiber structure and dimensions by AFM. The expected intercuboid gap is 21.6 nm, on the basis of the dimensions of Fn-III_{10} (3.8 nm, according to the crystal structure[28]) and the estimated lengths of the coiled-coils (4.2 nm) and dsDNA handles (4.7 nm); see Figure

https://doi.org/10.1021/acsabm.2c00303
ACS Appl. Bio Mater. XXXX, XXX, XXX−XXX

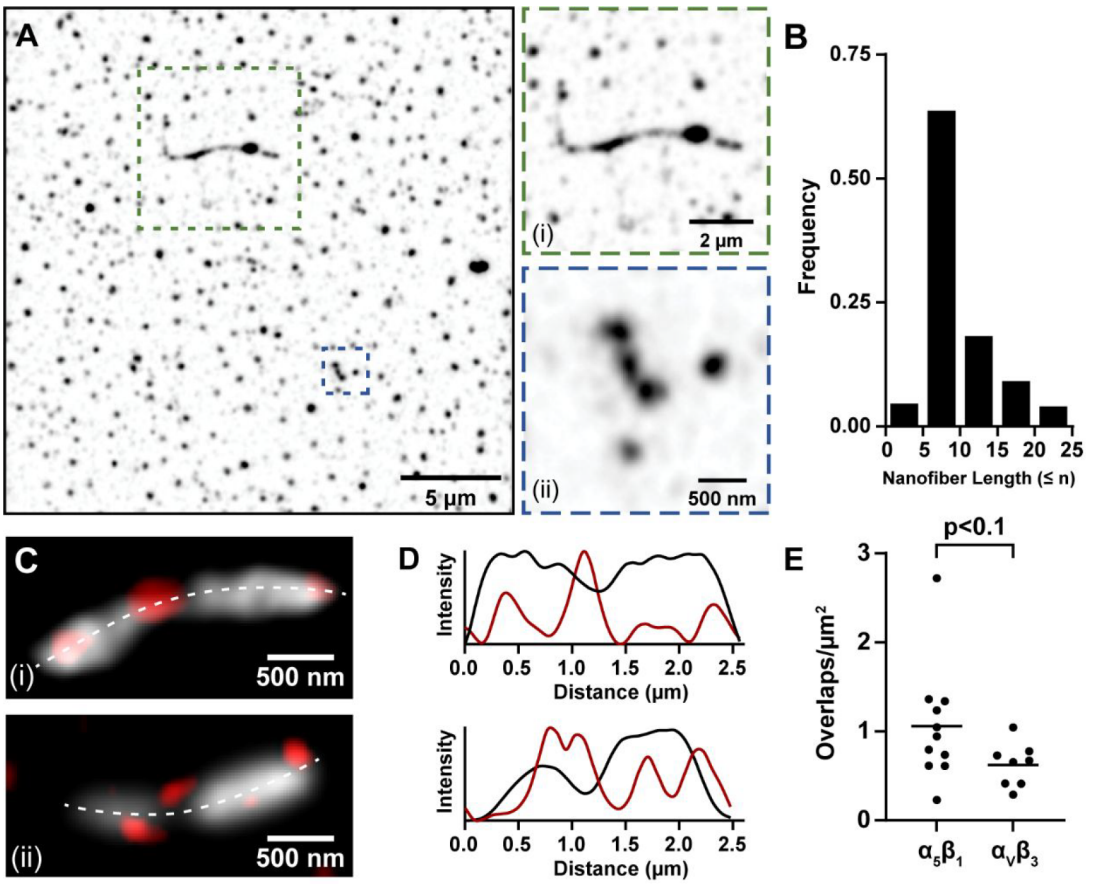

Figure 3. Modification of biocompatible surfaces with DNA−Fn-III$_{10}$ arrays. Glass substrates were modified with DNA−Fn-III$_{10}$ fibers and stained with YOYO-1, followed by imaging using CLSM. (A) A 25 × 25um overview image of the DNA−Fn-III$_{10}$ modified surface. Insets show areas representing long nanofiber (i) and shorter nanofiber (ii) arrays. (B) Quantification of fiber length from the confocal images. (C) Representative fibers containing regions of bound integrins, either $\alpha 5\beta 1$ (i) or $\alpha V\beta 3$ (ii). Gray = YOYO-1, DNA−nanofibers. Red = integrin (D) Line scans along the dotted lines in (C) show the overlapping regions of both DNA and integrins. Line-scan plots are shown normalized to the maximum value of a given trace. Black = YOYO-1 (DNA nanofibers). Red = integrin. (E) Quantification of the density of overlapping regions of integrin and DNA, representing regions of integrin binding. Mean overlap density shown by the bars.

S5. Combined with the dimensions of the long edge of the cuboid (32 nm), we expect a distance of 53.6 nm between the edges of each cuboid (Figure 2F), not taking into account the flexible linkers between the peptide and its DNA handle. AFM analysis of an isolated fiber (Figure 2G) demonstrated an average distance between the edges of adjacent cuboids of ∼53 nm (Figure 2H), which closely matches the expected value. Notably, this distance is greater than the previously measured intercuboid distance of ∼40 nm for the EI/KI$_N$ fibers,[23] as a result of the protein and the second coiled-coil pair between each cuboid in an array. The height and width of each individual cuboid are 11 and 24 nm, respectively (Figure 2I), as observed in the EI/KI$_N$ fibers. We note that these images were taken after drying on the mica substrate, so the cuboids are expected to be slightly flattened due to the drying effects. However, AFM analysis confirms that not only are the cuboids linked along the expected interface but also that the dimensions between them correlate well to the dimensions of the protein with the two coil handles.

In previous experiments with the EI/KI pair, the most efficient pathway for the assembly was to purify the cuboids first and then add a preformed coiled-coil/DNA conjugate to assemble them into fibers.[23] We thus explored whether annealing cuboids with P4 and KI peptides, purifying them, and only afterward adding a stoichiometric amount of P3−Fn-III$_{10}$−EI would lengthen the fiber assembly (Figure 2A, "purified cuboids (iii)" and "purified arrays (iv)"). By AGE, the purified cuboids (Figure 2J, lane (iii)) showed an aggregated band in the loading well, indistinguishable from the sample after the addition of the P3−Fn-III$_{10}$−EI linker and incubation at room temperature for 72 h (Figure 2J, lane (iv)). The examination of this species by AFM (Figure S19A), however, showed clustered cuboids, not long 1D arrays, which we attribute to nonspecific aggregation due to the spin concentration step. The sample after protein addition, in contrast, showed the expected arrays by AFM (Figures 2K,L and S19B). The quantification of the fiber length distribution (Figure 2M) showed a fairly similar distribution to the previous assembly protocol (Figure 2E), albeit with some longer fibers reaching 40 cuboids in length.

Having demonstrated successful assembly of nanofibers composed of DNA origami units linked by ECM-derived proteins, we next turned to probing the bioactivity of these fibers. We first needed to verify that they can efficiently modify glass surfaces for cell culture assays. As the DNA−Fn-III$_{10}$ fibers are assembled and purified in magnesium-containing solutions, they should efficiently bind to negatively charged plasma cleaned glass, as previously demonstrated.[29] To test this hypothesis, we applied solutions of DNA−Fn-III$_{10}$ fibers to glass coverslips immediately following plasma cleaning and

https://doi.org/10.1021/acsabm.2c00303
ACS Appl. Bio Mater. XXXX, XXX, XXX−XXX

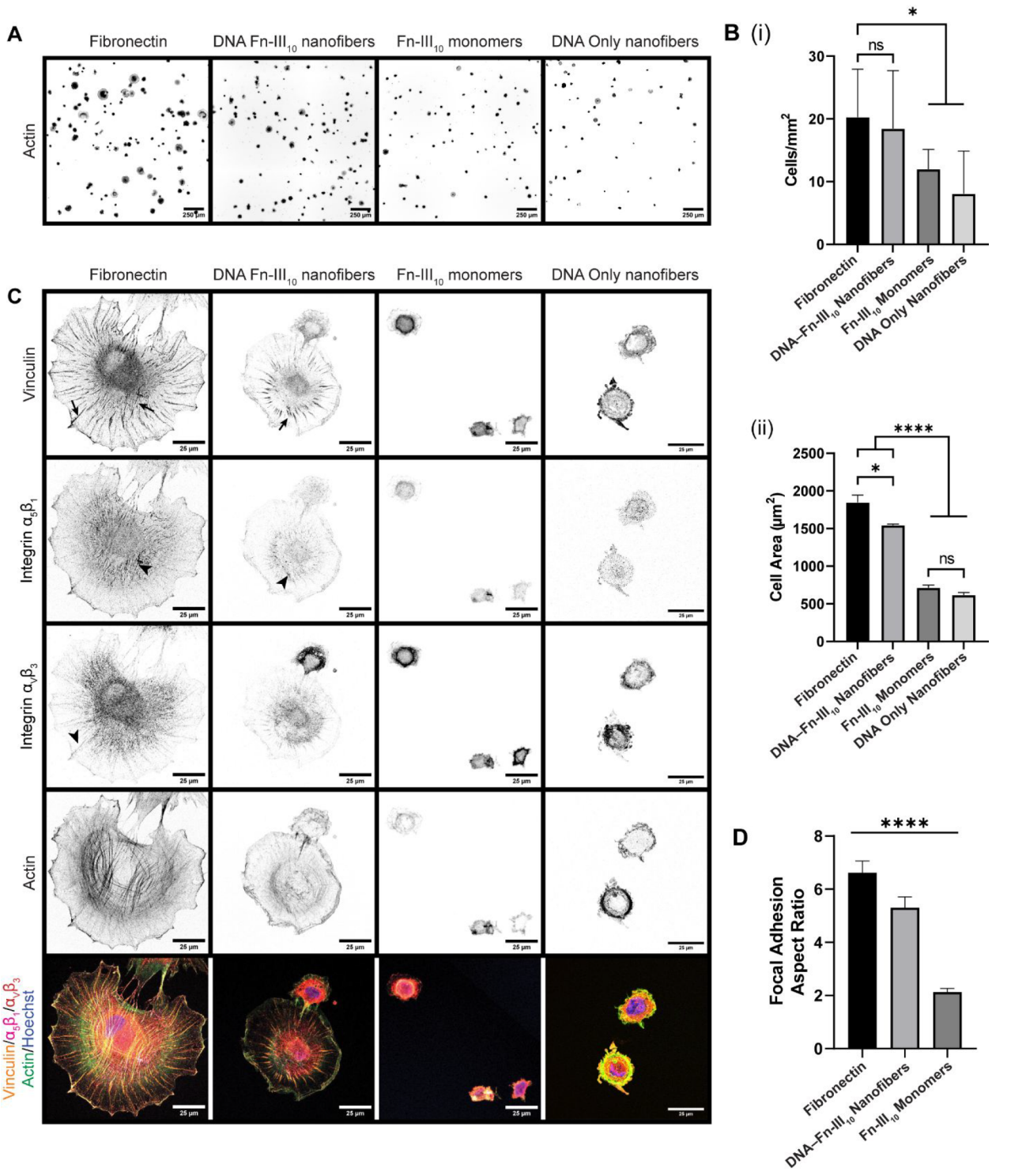

Figure 4. Cells adhesion and spreading on DNA−Fn-III$_{10}$ nanofibers. (A) Representative widefield images of cells grown on surfaces coated with native fibronectin, DNA−Fn-III$_{10}$ nanofibers, P3−Fn-III$_{10}$−EI monomers, or DNA-only nanofibers (10× objective, actin stained with AlexaFluor-phalloidin-488). (B) Quantification (from the brightfield images in (A)) of cell attachment density (i) and projected cell area (ii) on differently modified surfaces. (C) Confocal microscopy images of cells grown on the same surfaces stained for vinculin and integrins $a_5\beta_1$ and $a_V\beta_3$. Arrows: focal adhesions shown in the vinculin channel. Arrow heads: focal adhesions shown in the corresponding integrin channel. (D) Quantification (from the confocal images in (B)) of the vinculin channel showing the aspect ratio of focal adhesions larger than 0.5 μm^2 for cells grown on FN-containing surfaces. All error bars show the 95% confidence interval of the mean, and p-values were calculated in Prism using a one-way ANOVA. * = $p < 0.05$; **** = $p < 0.0001$.

allowed the functionalized surfaces to incubate at room temperature for 1 h, followed by two washes with Mg-supplemented PBS. To characterize the resulting surface coating, we used the DNA intercalator dye YOYO-1 to fluorescently label the DNA nanofibers, followed by imaging using confocal microscopy. This method of surface mod-

https://doi.org/10.1021/acsabm.2c00303
ACS Appl. Bio Mater. XXXX, XXX, XXX−XXX

ification resulted in the efficient coating of glass substrates with DNA−Fn-III$_{10}$ fibers 250−500 nm long, correlating well with the fiber length observed via AFM imaging (Figures 3A,B and S20). We next tested whether the Fn-III$_{10}$ domains within the hybrid fibers could effectively engage integrins. Glass surfaces modified with DNA−Fn-III$_{10}$ nanofibers were incubated with solutions of purified recombinant integrins, either $\alpha_5\beta_1$ or $\alpha_V\beta_3$, followed by labeling with primary antibodies against the corresponding integrin and fluorescent secondary antibodies. By labeling the DNA with YOYO-1, we were also able to visualize the spatial arrangement of integrins on the DNA nanofibers. This experiment revealed that both integrins were able to bind the DNA nanofibers (Figure 3Ci,ii). Line scans taken from representative images of integrin-bound DNA nanofibers (Figure 3D) revealed multiple points of overlap between the black (DNA) and red (integrin) signals with an apparent preference toward binding at the ends of the DNA fibers compared to the center. This may be because protein (either the Fn-III$_{10}$ domains themselves or the integrins to which the antibodies must bind) at the end of the fibers is more accessible, as there are no nanostructures on one side of them. Colocalization analysis of the imaged surfaces allowed us to quantify the density of these overlapping regions (Figures 3D and S21). Interestingly, the DNA−Fn-III$_{10}$ nanofibers revealed a slight binding preference toward integrin $\alpha5\beta1$ as shown by the increased number of overlaps/μm^2 (1.06 vs 0.62 μm^{-2}, $p < 0.1$). While the preference is mild, this result suggests it might be possible to design origami−Fn hybrids that would be selective toward target integrins.

Finally, we turned our efforts toward understanding whether these hybrid nanofibers could promote cell adhesion and spreading. We plated human foreskin fibroblasts (HFFs) on surfaces modified with either native fibronectin, DNA−Fn-III$_{10}$ nanofibers, or P3−Fn-III$_{10}$−EI protein monomers (Figure 4). Cells were allowed to adhere and spread under low serum conditions (2% FBS) for 2 h followed by fixation and staining. Images (10× magnification) of cells on these three surfaces (Figure 4A) were taken over the entire coverslip and used to quantify cell density and projected cell area. Cell density was variable across the surfaces, but the fibronectin and DNA−FN-III$_{10}$ surfaces showed an increased number of adhered cells. However, quantification of cell area revealed substantial differences (Figure 4Bi,ii). While the native fibronectin surfaces showed the highest degree of cell spreading (1848 ± 96 μm^2), cells on DNA−Fn-III$_{10}$ surfaces were significantly larger (1546 ± 14 μm^2) than on P3−Fn-III$_{10}$−EI surfaces (714 ± 36 μm^2, $p < 0.0001$). Cells on DNA−Fn-III$_{10}$ surfaces also showed significantly improved spreading compared to DNA-only nanofibers (619 ± 32 μm^2) or unmodified glass substrates (683 ± 39 μm^2, data not shown). We also performed immunocytochemistry labeling of cells on the differently modified surfaces and stained for proteins associated with focal adhesions (vinculin) and integrin activation ($\alpha5$ and $\beta3$ integrins) (Figure 4C). The cells grown on both native fibronectin and DNA−Fn-III$_{10}$ nanofibers show the formation of focal adhesions that are positive for both $\alpha5$ and $\beta3$ integrins. While these structures are not as mature in cells grown on DNA−Fn-III$_{10}$ nanofibers versus native Fn, the vinculin channel shows the formation of FAs that appear to be predominantly composed of integrin $\alpha5\beta1$, further suggesting a slight selectivity toward $\alpha5\beta1$, as we demonstrated in our binding studies (Figure 3). Interestingly, cells grown on the nonassembled P3−Fn-III$_{10}$−EI monomer only surfaces show very limited spreading and ill-defined structures in the vinculin and integrin channels. These differences were further characterized by quantifying the aspect ratio of the focal adhesions. Masks of the focal adhesions were isolated from the vinculin channel images and analyzed to calculate the mean FA aspect ratios, which were 6.71 ± 0.48, 5.31 ± 0.41, and 2.13 ± 0.14 for native Fn, DNA−Fn-III$_{10}$ nanofibers, and P3−Fn-III$_{10}$−EI monomer surfaces, respectively (Figure 4D). Taken together, these results suggest that, while the Fn-III$_{10}$ domain alone is sufficient to promote cell adhesion, the optimal engagement of integrins and effective cell spreading and focal adhesion formation require the Fn-III$_{10}$ domains to be polymerized via the DNA origami nanostructures. We further supported this by plating cells on surfaces with increasing concentrations of the P3−Fn-III$_{10}$−EI monomer either adsorbed or covalently linked to the surface. Both adsorbed and covalently linked monomers induced cell spreading (Figure S22A,B), but the covalently linked monomers caused a greater increase in cell area, once we controlled for the possible differences between the substrate and background (APTES vs plasma cleaned). Interestingly, although cells behaved differently on these modified surfaces, higher amounts of P3−Fn-III$_{10}$−EI monomer did not correlate with a higher degree of spreading, regardless of whether the monomer was covalently attached or not. This suggests that simply having more monomer on the surface is not sufficient to induce an efficient cell response. Instead, the ordered fibrillar geometry of the DNA nanofibers is needed to recreate the adhesion and spreading, and the possibly increased adhesion of the fibers to the surface compared with monomeric protein or cells responding partly to the nanomorphology of the fibers (vs globular monomeric proteins) is not sufficient. These questions will be the focus of future experiments with these hybrid systems. Our results highlight the importance of hierarchical ordering in ECM proteins, where the specific spatial and multivalent arrangement of bioactive cues is critical to achieve the desired cell activity.

CONCLUSIONS

In conclusion, we have demonstrated the synthesis of hybrid protein−DNA nanofibers that use two orthogonal coiled-coil pairs to assemble one-dimensional DNA origami nanostructures interspersed with bioactive Fn-III$_{10}$ domains. Furthermore, our method avoids having to chemically modify the protein with DNA handles and instead relies on standard genetic fusion techniques, simplifying protein incorporation into the DNA-based system. Our work is, to our knowledge, the first example of integrating proteins with a DNA nanostructure via the coiled-coil motif to create a hybrid self-assembled system. The programmability of the coiled-coil pairing rules[30,31] and the large toolkit of the orthogonal pairs make this self-assembly motif an attractive candidate for nanomaterials.[32−35] Although here we demonstrate only two orthogonal peptide interactions, this method should be readily extensible to the broad toolkit of specific coiled-coil pairs that have been previously described,[30,35] potentially enabling site-specific incorporation of multiple proteins.

We also demonstrated that fibers containing the proteins served as efficient scaffolds for cell adhesion and spreading with improved activity compared with monomeric proteins not assembled into a biomimetic fibrillar structure. The programmable nature of the underlying DNA origami backbone also allows for the incorporation of other domains within the same

https://doi.org/10.1021/acsabm.2c00303
ACS Appl. Bio Mater. XXXX, XXX, XXX−XXX

fiber, whether they are additional fibronectin domains or domains from other important ECM proteins. In addition, the nanoarray polymerization via DNA hybridization or coil–coiled interactions can be leveraged to make the fibers responsive and reconfigurable to user defined inputs through the use of both DNA and peptide strand displacement.[36,37] The ability to independently control the nanofiber morphology (e.g., aspect ratio, stiffness) and the number and identity of the proteins presented will enable structure–function studies for ECM-mimetic materials that are hard to accomplish using native proteins or other bioengineered systems like self-assembled all-peptide or protein nanofibers.

■ ASSOCIATED CONTENT

Supporting Information

The Supporting Information is available free of charge at https://pubs.acs.org/doi/10.1021/acsabm.2c00303.

Materials and supplies, peptide characterization, DNA sequences, protein expression plasmids and characterization, additional array characterization, additional details on fibroblast surface experiments, quantification of peptide–DNA conjugates on origami, and all DNA sequences used in the origami designs (PDF)

■ AUTHOR INFORMATION

Corresponding Authors

Ronit Freeman − *Department of Applied Physical Sciences, University of North Carolina, Chapel Hill, North Carolina 27514, United States;* orcid.org/0000-0001-5960-6689; Email: ronifree@email.unc.edu

Nicholas Stephanopoulos − *School of Molecular Sciences and Center for Molecular Design and Biomimetics, The Biodesign Institute, Arizona State University, Tempe, Arizona 85281, United States;* orcid.org/0000-0001-7859-410X; Email: nstepha1@asu.edu

Authors

Alex Buchberger − *School of Molecular Sciences and Center for Molecular Design and Biomimetics, The Biodesign Institute, Arizona State University, Tempe, Arizona 85281, United States;* orcid.org/0000-0003-3412-8945

Kyle Riker − *Department of Applied Physical Sciences, University of North Carolina, Chapel Hill, North Carolina 27514, United States;* orcid.org/0000-0003-4788-8687

Julio Bernal-Chanchavac − *School of Molecular Sciences and Center for Molecular Design and Biomimetics, The Biodesign Institute, Arizona State University, Tempe, Arizona 85281, United States*

Raghu Pradeep Narayanan − *School of Molecular Sciences and Center for Molecular Design and Biomimetics, The Biodesign Institute, Arizona State University, Tempe, Arizona 85281, United States*

Chad R. Simmons − *Center for Molecular Design and Biomimetics, The Biodesign Institute, Arizona State University, Tempe, Arizona 85281, United States;* orcid.org/0000-0002-2290-6132

Nour Eddine Fahmi − *Center for Molecular Design and Biomimetics, The Biodesign Institute, Arizona State University, Tempe, Arizona 85281, United States*

Complete contact information is available at: https://pubs.acs.org/10.1021/acsabm.2c00303

Author Contributions

‡A.B. and K.R. contributed equally.

Notes

The authors declare no competing financial interest.

■ ACKNOWLEDGMENTS

N.S. acknowledges startup funds from Arizona State University. This material is based upon work supported by the Air Force Office of Scientific Research under award number FA9550-17-1-0053. This work was supported by the National Science Foundation (DMR-BMAT CAREER award 1753387). Research reported in this publication was supported by The National Institute of General Medical Sciences of the National Institutes of Health under grant number DP2GM132931. The content is solely the responsibility of the authors and does not necessarily represent the official views of the National Institutes of Health. R.F. acknowledges support from the Alfred P. Sloan Foundation grant G-2021-14197.

■ REFERENCES

(1) Hong, F.; Zhang, F.; Liu, Y.; Yan, H. DNA Origami: Scaffolds for Creating Higher Order Structures. *Chem. Rev.* **2017**, *117* (20), 12584–12640.

(2) Seeman, N. C. At the crossroads of chemistry, biology, and materials: Structural DNA nanotechnology. *Chemistry & Biology* **2003**, *10* (12), 1151–1159.

(3) Rothemund, P. W. K. Folding DNA to create nanoscale shapes and patterns. *Nature* **2006**, *440* (7082), 297–302.

(4) MacCulloch, T.; Buchberger, A.; Stephanopoulos, N. Emerging applications of peptide-oligonucleotide conjugates: bioactive scaffolds, self-assembling systems, and hybrid nanomaterials. *Organic & Biomolecular Chemistry* **2019**, *17* (7), 1668–1682.

(5) Venkatesan, N.; Kim, B. H. Peptide conjugates of oligonucleotides: Synthesis and applications. *Chem. Rev.* **2006**, *106* (9), 3712–3761.

(6) Stephanopoulos, N. Hybrid Nanostructures from the Self-Assembly of Proteins and DNA. *Chem.* **2020**, *6* (2), 364–405.

(7) Sacca, B.; Niemeyer, C. M. Functionalization of DNA nanostructures with proteins. *Chem. Soc. Rev.* **2011**, *40* (12), 5910–5921.

(8) Madsen, M.; Gothelf, K. V. Chemistries for DNA Nanotechnology. *Chem. Rev.* **2019**, *119* (10), 6384–6458.

(9) Fang, T.; Alvelid, J.; Spratt, J.; Ambrosetti, E.; Testa, I.; Teixeira, A. I. Spatial Regulation of T-Cell Signaling by Programmed Death-Ligand 1 on Wireframe DNA Origami Flat Sheets. *ACS Nano* **2021**, *15* (2), 3441–3452.

(10) Huang, D.; Patel, K.; Perez-Garrido, S.; Marshall, J. F.; Palma, M. DNA Origami Nanoarrays for Multivalent Investigations of Cancer Cell Spreading with Nanoscale Spatial Resolution and Single-Molecule Control. *ACS Nano* **2019**, *13* (1), 728–736.

(11) Hawkes, W.; Huang, D.; Reynolds, P.; Hammond, L.; Ward, M.; Gadegaard, N.; Marshall, J. F.; Iskratsch, T.; Palma, M. Probing the nanoscale organisation and multivalency of cell surface receptors: DNA origami nanoarrays for cellular studies with single-molecule control. *Faraday Discuss.* **2019**, *219*, 203–219.

(12) Hellmeier, J.; Platzer, R.; Eklund, A. S.; Schlichthaerle, T.; Karner, A.; Motsch, V.; Schneider, M. C.; Kurz, E.; Bamieh, V.; Brameshuber, M. DNA origami demonstrate the unique stimulatory power of single pMHCs as T cell antigens. *Proc. Natl. Acad. Sci. U. S. A.* **2021**, *118* (4), e2016857118.

(13) Kern, N.; Dong, R.; Douglas, S. M.; Vale, R. D.; Morrissey, M. A. Tight nanoscale clustering of Fcγ receptors using DNA origami promotes phagocytosis. *eLife* **2021**, *10*, e68311.

(14) Dutta, P. K.; Zhang, Y.; Blanchard, A. T.; Ge, C.; Rushdi, M.; Weiss, K.; Zhu, C.; Ke, Y.; Salaita, K. Programmable Multivalent DNA-Origami Tension Probes for Reporting Cellular Traction Forces. *Nano Lett.* **2018**, *18* (8), 4803–4811.

(15) Aldaye, F. A.; Senapedis, W. T.; Silver, P. A.; Way, J. C. A Structurally Tunable DNA-Based Extracellular Matrix. *J. Am. Chem. Soc.* **2010**, *132* (42), 14727−14729.
(16) Stephanopoulos, N.; Freeman, R.; North, H. A.; Sur, S.; Jeong, S. J.; Tantakitti, F.; Kessler, J. A.; Stupp, S. I. Bioactive DNA-Peptide Nanotubes Enhance the Differentiation of Neural Stem Cells Into Neurons. *Nano Lett.* **2015**, *15* (1), 603−609.
(17) Singh, P.; Carraher, C.; Schwarzbauer, J. E. Assembly of Fibronectin Extracellular Matrix. *Annual Review of Cell and Developmental Biology* **2010**, *26* (26), 397−419.
(18) Bernfield, M.; Götte, M.; Park, P. W.; Reizes, O.; Fitzgerald, M. L.; Lincecum, J.; Zako, M. Functions of Cell Surface Heparan Sulfate Proteoglycans. *Annu. Rev. Biochem.* **1999**, *68* (1), 729−777.
(19) Martino, M. M.; Tortelli, F.; Mochizuki, M.; Traub, S.; Ben-David, D.; Kuhn, G. A.; Mueller, R.; Livne, E.; Eming, S. A.; Hubbell, J. A. Engineering the Growth Factor Microenvironment with Fibronectin Domains to Promote Wound and Bone Tissue Healing. *Science Translational Medicine* **2011**, *3* (100), 100ra89.
(20) Martino, M. M.; Hubbell, J. A. The 12th-14th type III repeats of fibronectin function as a highly promiscuous growth factor-binding domain. *Faseb Journal* **2010**, *24* (12), 4711−4721. Mardon, H. J.; Grant, K. E. THE ROLE OF THE 9TH AND 10TH TYPE-III DOMAINS OF HUMAN FIBRONECTIN IN CELL-ADHESION. *Febs Letters* **1994**, *340* (3), 197−201.
(21) Engler, A. J.; Sen, S.; Sweeney, H. L.; Discher, D. E. Matrix elasticity directs stem cell lineage specification. *Cell* **2006**, *126* (4), 677−689.
(22) Tigges, T.; Heuser, T.; Tiwari, R.; Walther, A. 3D DNA Origami Cuboids as Monodisperse Patchy Nanoparticles for Switchable Hierarchical Self-Assembly. *Nano Lett.* **2016**, *16* (12), 7870−7874.
(23) Buchberger, A.; Simmons, C. R.; Fahmi, N. E.; Freeman, R.; Stephanopoulos, N. Hierarchical Assembly of Nucleic Acid/Coiled-Coil Peptide Nanostructures. *J. Am. Chem. Soc.* **2020**, *142* (3), 1406−1416.
(24) Gradisar, H.; Jerala, R. De novo design of orthogonal peptide pairs forming parallel coiled-coil heterodimers. *Journal of Peptide Science* **2011**, *17* (2), 100−106.
(25) Aronsson, C.; Danmark, S.; Zhou, F.; Oberg, P.; Enander, K.; Su, H.; Aili, D. Self-sorting heterodimeric coiled coil peptides with defined and tuneable self-assembly properties. *Sci. Rep.* **2015**, *5*, 10.1038/srep14063.
(26) Frank, A. O.; Otto, E.; Mas-Moruno, C.; Schiller, H. B.; Marinelli, L.; Cosconati, S.; Bochen, A.; Vossmeyer, D.; Zahn, G.; Stragies, R.; Novellino, E.; Kessler, H. Conformational control of integrin-subtype selectivity in isoDGR peptide motifs: a biological switch. *Angew. Chem., Int. Ed.* **2010**, *49* (48), 9278−9281.
(27) Kapp, T. G.; Rechenmacher, F.; Neubauer, S.; Maltsev, O. V.; Cavalcanti-Adam, E. A.; Zarka, R.; Reuning, U.; Notni, J.; Wester, H. J.; Mas-Moruno, C.; Spatz, J.; Geiger, B.; Kessler, H. A comprehensive evaluation of the activity and selectivity profile of ligands for RGD-binding integrins. *Sci. Rep.* **2017**, *7* (1), 1−13.
(28) Dickinson, C. D.; Veerapandian, B.; Dai, X.-P.; Hamlin, R. C.; Xuong, N.-H.; Ruoslahti, E.; Ely, K. R. Crystal structure of the tenth type III cell adhesion module of human fibronectin. *J. Mol. Biol.* **1994**, *236*, 1079−1092.
(29) Kapp, T. G.; Rechenmacher, F.; Neubauer, S.; Maltsev, O. V.; Cavalcanti-Adam, E. A.; Zarka, R.; Reuning, U.; Notni, J.; Wester, H.-J.; Mas-Moruno, C.; Spatz, J.; Geiger, B.; Kessler, H. A Comprehensive Evaluation of the Activity and Selectivity Profile of Ligands for RGD-binding Integrins. *Sci. Rep.* **2017**, *7* (1), 39805.
(30) Wood, C. W.; Bruning, M.; Ibarra, A. A.; Bartlett, G. J.; Thomson, A. R.; Sessions, R. B.; Brady, R. L.; Woolfson, D. N. CCBuilder: an interactive web-based tool for building, designing and assessing coiled-coil protein assemblies. *Bioinformatics* **2014**, *30* (21), 3029−3035.
(31) Apostolovic, B.; Danial, M.; Klok, H. A. Coiled coils: attractive protein folding motifs for the fabrication of self-assembled, responsive and bioactive materials. *Chem. Soc. Rev.* **2010**, *39* (9), 3541−3575.
(32) Fletcher, J. M.; Harniman, R. L.; Barnes, F. R. H.; Boyle, A. L.; Collins, A.; Mantell, J.; Sharp, T. H.; Antognozzi, M.; Booth, P. J.; Linden, N.; Miles, M. J.; Sessions, R. B.; Verkade, P.; Woolfson, D. N. Self-Assembling Cages from Coiled-Coil Peptide Modules. *Science* **2013**, *340* (6132), 595−599.
(33) Banwell, E. F.; Abelardo, E. S.; Adams, D. J.; Birchall, M. A.; Corrigan, A.; Donald, A. M.; Kirkland, M.; Serpell, L. C.; Butler, M. F.; Woolfson, D. N. Rational design and application of responsive alpha-helical peptide hydrogels. *Nat. Mater.* **2009**, *8* (7), 596−600.
(34) Pandya, M. J.; Spooner, G. M.; Sunde, M.; Thorpe, J. R.; Rodger, A.; Woolfson, D. N. Sticky-end assembly of a designed peptide fiber provides insight into protein fibrillogenesis. *Biochemistry* **2000**, *39* (30), 8728−8734.
(35) Gradisar, H.; Bozic, S.; Doles, T.; Vengust, D.; Hafner-Bratkovic, I.; Mertelj, A.; Webb, B.; Sali, A.; Klavzar, S.; Jerala, R. Design of a single-chain polypeptide tetrahedron assembled from coiled-coil segments. *Nat. Chem. Biol.* **2013**, *9* (6), 362−366.
(36) Freeman, R.; Stephanopoulos, N.; Alvarez, Z.; Lewis, J. A.; Sur, S.; Serrano, C. M.; Boekhoven, J.; Lee, S. S.; Stupp, S. I. Instructing cells with programmable peptide DNA hybrids. *Nat. Commun.* **2017**, *8*, 15982.
(37) Riker, K. D.; Daly, M. L.; Papanikolas, M. J.; Jian, T.; Klawa, S. J.; Shin (Sahin), J. Y. S.; Liu, D.; Singh, A.; Miller, A. G.; Freeman, R. A Programmable Toolkit to Dynamically Signal Cells Using Peptide Strand Displacement. *ACS Appl. Mater. Interfaces* **2021**, *13* (18), 21018−21029.

https://doi.org/10.1021/acsabm.2c00303
ACS Appl. Bio Mater. XXXX, XXX, XXX−XXX